Article

Cell Host & Microbe

Influenza Antigen Engineering Focuses Immune Responses to a Subdominant but Broadly Protective Viral Epitope

Graphical Abstract

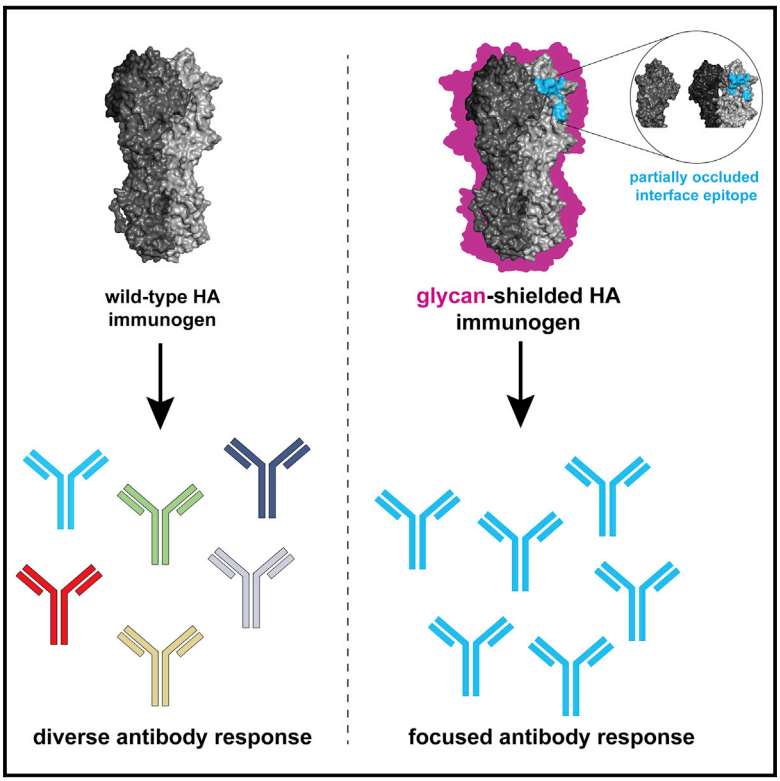

Authors

Goran Bajic, Max J. Maron, Yu Adachi, ..., Garnett Kelsoe, Masayuki Kuraoka, Aaron G. Schmidt

Correspondence

masayuki.kuraoka@duke.edu (M.K.), aschmidt@crystal.harvard.edu (A.G.S.)

In Brief

Eliciting protective immunity against influenza remains a major challenge. Bajic et al. show how hemagglutinin (HA) hyperglycosylation can restrict the resulting antibody repertoire to an occluded epitope at the HA head interface. These antibodies protect against influenza-virus challenge, providing insights into antigen engineering to alter antibody responses.

Highlights

- Hyperglycosylation of hemagglutinin (HA) does not dampen serum and GC responses
- Hyperglycosylation of HA changes patterns of immunodominance
- Glycan addition restricts antibody repertoire to a subdominant epitope
- Antibodies targeting this occluded epitope on HA protect against viral challenge

Bajic et al., 2019, Cell Host & Microbe *25*, 1–9
June 12, 2019
https://doi.org/10.1016/j.chom.2019.04.003

CellPress

Please cite this article in press as: Bajic et al., Influenza Antigen Engineering Focuses Immune Responses to a Subdominant but Broadly Protective Viral Epitope, Cell Host & Microbe (2019), https://doi.org/10.1016/j.chom.2019.04.003

Cell Host & Microbe
Article

Influenza Antigen Engineering Focuses Immune Responses to a Subdominant but Broadly Protective Viral Epitope

Goran Bajic,[1,7] Max J. Maron,[2,7] Yu Adachi,[3] Taishi Onodera,[3] Kevin R. McCarthy,[1] Charles E. McGee,[4] Gregory D. Sempowski,[4] Yoshimasa Takahashi,[3] Garnett Kelsoe,[4,5] Masayuki Kuraoka,[5,*] and Aaron G. Schmidt[2,6,8,*]
[1]Laboratory of Molecular Medicine, Boston Children's Hospital, Harvard Medical School, Boston, MA 02115, USA
[2]Ragon Institute of MGH, MIT and Harvard, Cambridge, MA 02139, USA
[3]Department of Immunology, National Institute of Infectious Diseases, Tokyo 162-8640, Japan
[4]Duke Human Vaccine Institute, Duke University, Durham, NC 27710, USA
[5]Department of Immunology, Duke University, Durham, NC 27710, USA
[6]Department of Microbiology, Harvard Medical School, Boston, MA 02115, USA
[7]These authors contributed equally
[8]Lead Contact
*Correspondence: masayuki.kuraoka@duke.edu (M.K.), aschmidt@crystal.harvard.edu (A.G.S.)
https://doi.org/10.1016/j.chom.2019.04.003

SUMMARY

Viral glycoproteins are under constant immune surveillance by a host's adaptive immune responses. Antigenic variation including glycan introduction or removal is among the mechanisms viruses have evolved to escape host immunity. Understanding how glycosylation affects immunodominance on complex protein antigens may help decipher underlying B cell biology. To determine how B cell responses can be altered by such modifications, we engineered glycans onto the influenza virus hemagglutinin (HA) and characterized the molecular features of the elicited humoral immunity in mice. We found that glycan addition changed the initially diverse antibody repertoire into an epitope-focused, genetically restricted response. Structural analyses showed that one antibody gene family targeted a previously subdominant, occluded epitope at the head interface. Passive transfer of this antibody conferred Fc-dependent protection to influenza virus-challenged mice. These results have potential implications for next-generation viral vaccines aimed at directing B cell responses to preferred epitope(s).

INTRODUCTION

An outstanding question in adaptive immunity is why particular epitopes on an antigen are preferentially targeted by antibodies (Abs); moreover, why the magnitude and genetic diversity of the elicited antibody response vary among epitopes on a complex antigen. This phenomenon, better known as immunodominance, represents a significant hurdle for next-generation vaccines against rapidly evolving pathogens such as influenza and HIV. Indeed, analyses of antibody repertoires elicited against influenza hemagglutinin (HA) and HIV envelope (Env) glycoproteins, both major targets of the adaptive immune response, show that the immunodominant responses often target variable epitopes, which mutate readily to allow pathogen escape (Wrammert et al., 2008). The broadly protective responses are generally subdominant, target conserved epitopes, such as a receptor-binding site (RBS), with limited variability because of functional constraints, and often show restricted gene usage (Petrova and Russell, 2018). Thus, we need to understand the molecular correlates of immunodominance, in order to meet the challenge of directing immune responses away from antigenically variable epitopes to ordinarily subdominant but less variable and more broadly protective ones.

Strategies to alter patterns of immunodominance often focus on rational immunogen design approaches aimed at eliciting broadly neutralizing antibodies (bnAbs) (Correia et al., 2014; Haynes et al., 2012; Jardine et al., 2015; Mascola and Haynes, 2013). A substantial number of bnAbs have been identified targeting conserved, subdominant epitopes on viral envelope glycoproteins. For both influenza HA and HIV Env, bnAbs have been isolated that target the conserved viral RBS as well as the membrane proximal region (MPER) in gp41 and an equivalent so-called "stem" region of HA (Corti et al., 2011; Ekiert et al., 2012; Krause et al., 2011; McCarthy et al., 2018; Schmidt et al., 2015b). Several different approaches have been taken to engineer immunogens that selectively present these and other conserved epitopes. For example, computational design approaches have produced novel scaffolds that present a single alpha helix derived from HIV and respiratory syncytial virus (RSV) glycoproteins (Correia et al., 2014; Ofek et al., 2010). Deconstructing the viral glycoprotein into domain-only fragments has yielded candidate immunogens containing the subdominant epitope(s) (Krammer and Palese, 2015). The underlying premise of these strategies is to entirely remove the immunodominant epitope(s) from the immunogen, in order to elicit broadly neutralizing responses focused on conserved but subdominant epitopes.

An alternative approach for changing immunodominance is to shield immunodominant epitope(s). Viral evolution has naturally explored introducing or removing glycans to reduce or evade host adaptive immune responses (Lavie et al., 2018; Watanabe et al., 2018). On one extreme, HIV Env protein has an average of 25 glycans per subunit, accounting for nearly half of its molecular

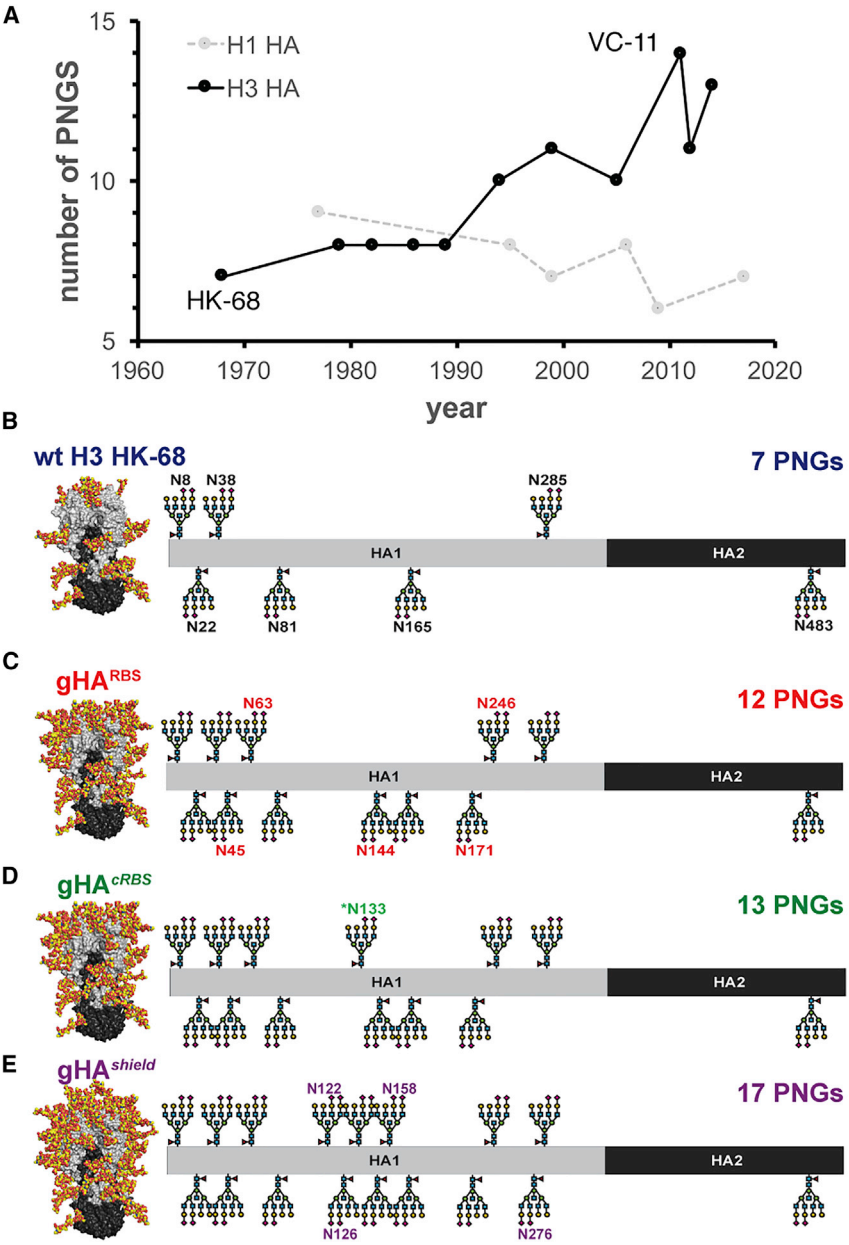

Figure 1. HA Glycan Evolution and Construct Design

(A) Number of putative N-linked glycans (PNGs) of historical H1 (gray, dashed line) and H3 (solid, black line) HAs beginning from 1977 and 1968, respectively. The template immunogen, H3 Hong Kong/1/1968 (HK-68) and the natively most glycosylated, H3 Victoria/361/2011 (VC-11), are noted.

(B) The WT H3 HK-68 with its native glycans are marked.

(C) gHA^{RBS} with additional glycans marked in red.

(D) gHA^{cRBS} with additional glycans marked in green.

(E) gHA^{shield} with additional glycans marked in purple.

The total number of glycans for each construct is noted. See also Figure S1.

mass, thus creating a so-called "glycan shield" (Crispin et al., 2018), while flaviviruses, like dengue, have only one or two conserved glycans per subunit (Modis et al., 2003, 2005). Influenza HA has a more varied glycosylation profile, depending on the subtype, which ranges between 7 and 14 glycans per polypeptide chain of the HA_0 precursor. Thus, for those viruses whose glycoproteins are hypoglycosylated, increasing glycan density may direct immune responses to subdominant epitopes and provide insight into how antibody repertoires change in response to glycosylation. We used influenza HA as a model antigen to query the impact of its altered glycosylation profile onto the amplitude and focus of host immune responses. We found that glycan shielding, believed to be responsible for poor immunogenicity of many pathogens and vaccine candidates including HIV Env, had no significant impact on the amplitude of humoral immune responses including serum antibody and germinal center (GC) reactions. In contrast to wild-type (WT) HA, the hyperglycosylated HAs elicited restricted V_H-gene responses, reminiscent of hapten-induced ones. Of these restricted responses, we discovered a class of subdominant Abs targeting a conserved, occluded epitope that becomes dominant after hyperglycosylation. We show that an antibody from this class did not neutralize *in vitro* but conferred complete protection *in vivo* after a lethal influenza challenge. These data show that glycan engineering of a viral antigen can change patterns of immunodominance and focus immune responses to broadly protective epitopes often occluded in the native protein oligomer.

RESULTS

Design and Characterization of Glycan-Modified Hemagglutinins

We took the following approach to identify potential sites for glycan modification using H3 Hong Kong/1/1968 (HK-68) HA from group 2 influenza as the template. We analyzed H3s circulating in the human population since 1968 and identified native, putative N-linked glycosylation sites (PNGs) on HA that could be engineered into HK-68. While circulating H1s have maintained an average of 8 PNGs since 1977, H3s have doubled the number of PNGs from 7 to 14 during their evolution in humans from 1968 to the present (Figures 1A and 1B). After glycan modeling of these native PNGs and identifying potential "glycan holes," we added non-native PNGs. Implementing these approaches resulted in three glycan-modified hemagglutinins (gHAs): gHA^{RBS}, gHA^{cRBS}, and gHA^{shield}. The first has an exposed RBS. The second has an additional PNG that prevents RBS-directed Abs from binding ("concealed" RBS: *cRBS*). The third creates a glycan "shield" covering all surface-exposed epitopes (Figures 1C–1E). We expressed all constructs in mammalian cells to

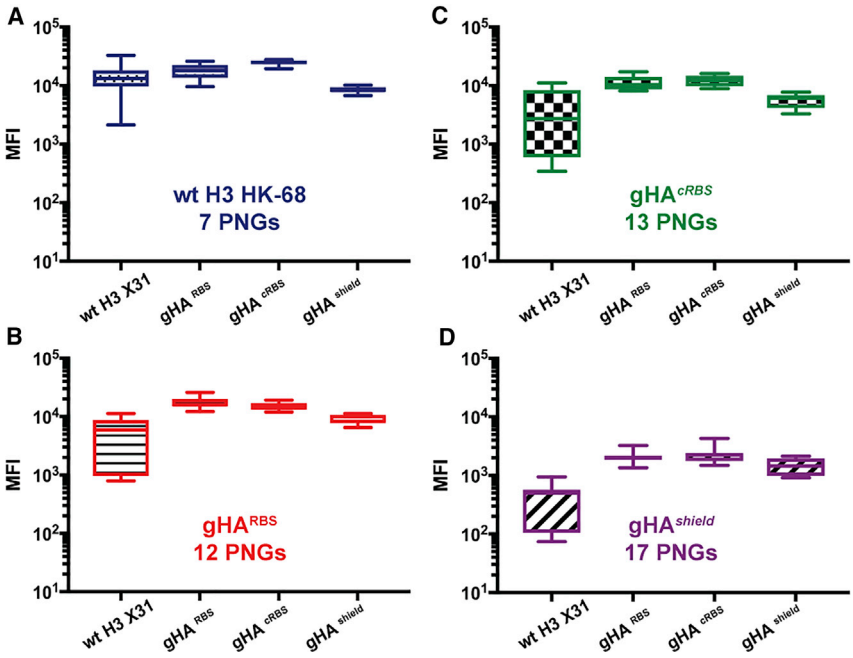

Figure 2. Amplitude of Antibody Serum Responses Is Unaffected by HA Glycosylation

C57BL/6J (B6) mice were immunized with WT H3 HK-68 (n = 7), gHA^{RBS} (n = 6), gHA^{cRBS} (n = 6), or gHA^{shield} (n = 4) and bled 16 days post-immunization. The sera were screened for binding to (A) WT H3 HK-68, (B) gHA^{RBS}, (C) gHA^{cRBS}, and (D) gHA^{shield} in a Luminex-based assay. Mean fluorescence intensity (MFI) signal ± SD is reported; n = number of mice used. See also Figure S2.

ensure complex glycosylation. Successful glycan addition was assayed by loss of reactivity to a panel of conformational-specific Abs, HC19, HC45, and FI6, whose epitopes overlap some of the engineered PNGs (Figure S1).

Immunogenicity of Glycan-Modified Hemagglutinins

We tested sera taken at day 8 or day 16 post immunization from mice administered WT HK-68, gHA^{RBS}, gHA^{cRBS}, or *gHA^{shield}* for reactivity to WT HK-68 and each of the gHAs (Figures 2A–2D). We found that serum IgGs from each gHA immunization bound WT HK-68 as well as the control serum IgGs from WT HK-68 immunization. These data suggest that few, if any, serum IgG responses required interaction with the introduced glycans for binding. Additionally, each gHA serum cross-reacted with each gHA construct, suggesting a shared serum response elicited by each gHA that was unaffected by the increasing number of glycans. Indeed, even WT HK-68 immunization had a serum response that reacted with each of the gHA constructs—including gHA^{shield}. Since gHA^{cRBS} and gHA^{shield} blocked binding of the RBS-directed HC19, the observed reactivity was probably to an epitope, or epitopes, outside the canonical RBS-directed Ab footprint. To complement our serological characterization, we assessed the reactivity of individual GC B cells isolated post immunization, using our single-cell Nojima culture system. By screening culture supernatants from each gHA immunization against the other three gHAs and WT HK-68, we found that the single-B cell reactivity profiles validated our epitope masking strategy: only a handful of GC B cell clones elicited by WT HK-68 immunization bound either of the gHA immunogens (Figures 3A and S3A). More importantly, while elicited by increasingly glycosylated HA immunogens, all of the responding GC B cells still bound the WT HK-68 (Figures 3B–3D and S2B–S2D). These data indicate that no glycan-specific responses were elicited by gHAs and that the gHA responses targeted hitherto undescribed, common HA epitopes. Furthermore, the gHAs elicited equally robust GC and plasmablast responses (Figures S2E and S2F). Thus, increasing the number of glycans on HA trimers did not impair the overall magnitude of humoral responses in mice.

Genetically Restricted V_H-Gene Usages in Responses to Glycan-Modified Hemagglutinins

We previously found that complex antigens, such as an HA from group 1 H1 Solomon Islands/03/2006 (H1 SI-06), elicited genetically diverse, unrestricted GC B cell responses (Kuraoka et al., 2016); complex antigens thus differ from haptens, which often produce stereotyped immune responses. Consistent with this observation, immunization with group 2 WT HA H3 HK-68 similarly elicited a genetically diverse and non-stereotyped response (Figure 4A). In contrast, however, the V_H-gene usage narrowed dramatically upon immunization with the gHAs, selectively enriching for three V_H genes: 1-69, 1-9, and 5-9-1 (Figures 4B–4D). V_H1-9 accounted for approximately 50% of the isolated, single-GC B cell-derived Abs to both gHA^{RBS} (37/69) (Figure 4B) and gHA^{cRBS} (39/81) (Figure 4C), but was absent from the response to WT HK-68 HA and reduced to ~7% (4/56) in gHA^{shield} (Figure 4C). Of the isolated V_H1-9 Abs, a substantial number were clonally related as determined by the relatedness of their heavy chain complementarity-determining region 3 (CDR H3); we identified a total of 9 unique lineages, with the largest clone containing 20 members from gHA^{cRBS} immunization. V_H1-69 was the next most abundant gene segment in the responses to gHA^{RBS} and gHA^{shield}; the frequency of this response in animals receiving the hyperglycosylated HAs was also greater than its level in the response to WT HA HK-68. We identified 9 lineages and 5 orphan Abs from this gene family. Lastly, V_H5-9-1 accounted for ~10% of the gHA^{RBS} and gHA^{shield} responses and paired with the rare lambda-light chain; this gene usage increased in frequency from ~0.7% (1/137) in response to WT HK-68 HA immunization. These data show that glycan-modified HAs elicited greatly enhanced frequencies of preferred V_H-gene usages.

Reactivity Profiles and Epitope Mapping of Stereotyped V_H-Gene Responses

We next obtained cross-reactivity profiles for each stereotyped V_H-gene response to WT HA, gHA^{RBS}, or gHA^{cRBS} and gHA^{shield} (Figure S3). The V_H1-9 group of Abs bound gHA^{cRBS} and WT HA but failed to react with gHA^{shield}; the latter result is consistent with the lack of enrichment of this V_H gene by gHA^{shield}

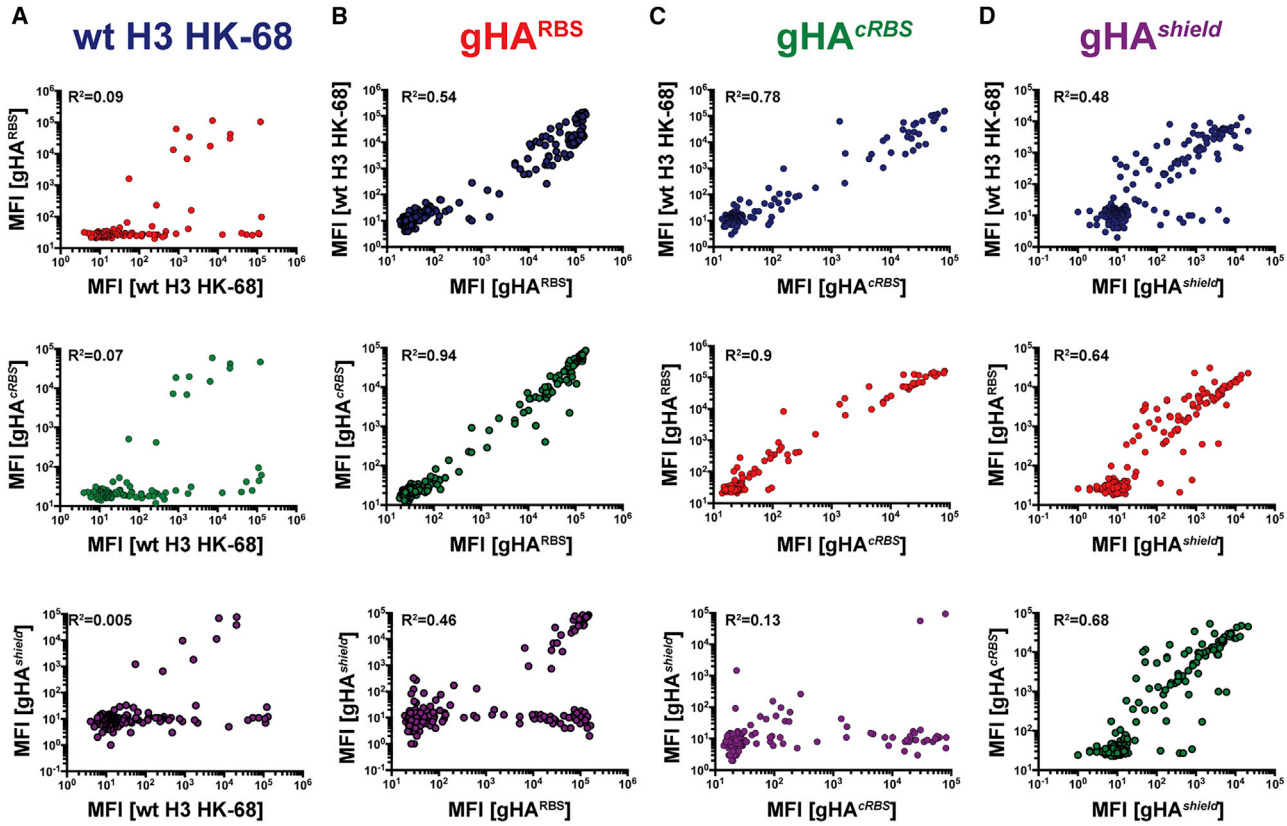

Figure 3. Single-Cell Cultures Reveal Differences in Antibody Epitopes Elicited by gHAs

Single-GC B cells were sorted from the popliteal lymph nodes of immunized B6 mice and cultured with NB-21.2D9 feeder cells. Individual single-cell culture supernatants from mice immunized with (A) WT H3 HK-68 (blue, n = 150), (B) gHA^{RBS} (red, n = 268), (C) gHA^{cRBS} (green, n = 177), and (D) gHA^{shield} (purple, n = 245) were harvested and screened for binding in a Luminex-based assay. The binding signal to the immunizing antigen (x axis) was compared to the other three HA immunogen constructs (y axis). The coefficient of determination (R^2) of a linear regression fit is reported. n = number of monoclonal Abs from supernatants used in screening. See also Figure S3.

immunizations (Figure S3A). Both the V_H1-69 and 5-9-1 classes of Abs cross-reacted with all constructs despite only being enriched in the gHA^{RBS} and gHA^{shield} immunizations (Figure S3B). Because all Abs elicited by the gHA immunizations bind WT HA HK-68, these data suggest that, while the epitope may include glycan interactions, antibody binding did not depend critically on the introduced glycans. We tested V_H5-9-1 Abs, 8H10 elicited by the WT HK-68 immunization, and FL-1066 from gHA^{shield} immunization, for binding against a panel of historical H3 HAs spanning over 30 years of antigenic drift. We found that 8H10 and FL-1066 were broadly reactive with historical H3s; additionally, both Abs bound a representative H4 (Figure S4A).

V_H5-9-1 Abs Recognize an Ordinarily Occluded Epitope

We determined crystal structures of three V_H5-9-1 Abs (Table S1)—an antibody elicited by WT HK-68 immunization, 8H10 (Figure 5A), and two members of two distinct antibody lineages arising from gHA^{RBS} immunization, FL-1056, and FL-1066 (Figures 5B and 5C). The 8H10 antibody was determined in complex with a variant of H4 A/America black duck/New Brunswick/00464/2010 HA and the other Abs in complex with H3 HK-68. The structures showed that all three Abs converged to bind the same epitope on the HA head. The Abs contacted a lateral surface of the HA head that is engaged in the interface between two HA protomers of a trimer (Figure S5). Thus, most of the epitope is occluded on a pre-fusion structure of an HA trimer. The antigen-combining site included contributions of both the heavy- and the light-CDR loops. The interaction interface was largely hydrophobic and the main interfacing amino-acid residues on HA were Pro221 and Trp222 (Pro217 and Trp222 on an H4). On the antibody side, the CDRs provided aromatic side-chain residues that sandwiched the HA Pro221 and Trp222 in a hydrophobic cleft between the light- and the heavy-chain CDRs (Figures 5A–5C). The conservation of this tryptophan between historical H3s and H4 helps explain, in part, the broad reactivity of these V_H5-9-1 Abs. Because of the occluded nature of the epitope, we performed cell surface-expressed H3 and H4 HA binding by flow cytometry (Figures S4B and S4C) and to intact H3 virions (Figure S4D). Both assays confirmed that these Abs can indeed engage an intact trimeric HA.

V_H5-9-1 Abs Are Non-neutralizing but Confer Fc-Dependent Protection *In Vivo*

We carried out *in vivo* protection studies in mice to determine if V_H5-9-1 Abs could mediate protection against a lethal challenge

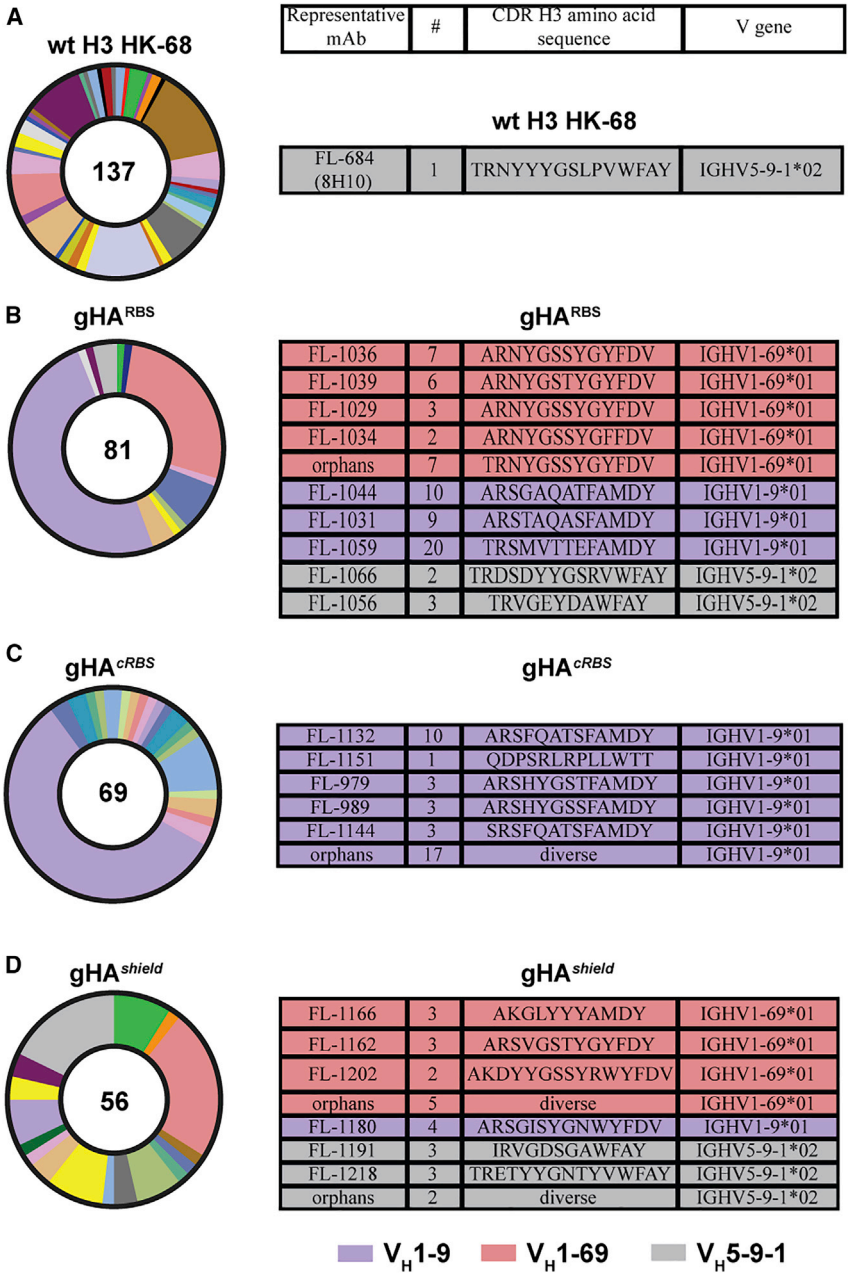

Figure 4. Adaptive Immune Responses to gHAs Are Genetically Restricted in Contrast to the WT HA

V_H gene usage frequencies in B6 mice immunized with (A) WT H3 HK-68, (B) gHA^{RBS}, (C) gHA^{cRBS}, and (D) gHA^{shield} shown as pie charts with the total number of GC B cells marked in the center of the charts. The three major V_H gene (IGHV1-9 [purple], 1-69 [pink], and 5-9-1 [gray]) family members are highlighted and reported in a table summarizing their clonotypes (as defined by their CDR H3 loops) and the number (#) of members in each lineage. See also Figure S4.

with influenza viruses. Passive transfer of a murine IgG1 version of 8H10 conferred limited protection against 5× LD_{50} intranasal challenge by H3N2 X31 (Figures 6A and 6B), but the murine IgG2c version of 8H10 conferred complete protection against the same challenge regimen. The results indicate that an Fc-dependent mechanism was responsible for protection. This observation is consistent with a lack of *in vitro* neutralizing activity against H3N2 in a microneutralization assay with 8H10 (Figure 6C).

DISCUSSION

We showed here that host immune responses can be manipulated through altering glycan density on influenza HA. We discovered a class of V_H5-9-1 restricted Abs that recognized a conserved, cryptic epitope of influenza HAs. These clonally unrelated Abs converged in their mode of antigen recognition and bound the occluded HA epitope in a similar fashion. These V_H5-9-1 Abs were broad within the H3 subtype, from which the gHA immunogens are based, but also recognized the potentially pre-pandemic H4 subtype. While a representative antibody from this class did not neutralize *in vitro*, it did protect mice against lethal challenge with an H3 subtype virus in an Fc-dependent manner. An objective of this study was to use glycan engineering to focus the murine response to the RBS. The gHA^{RBS}, with an exposed RBS, did not significantly increase RBS-directed responses however, and it appears that this site remained poorly immunogenic in mice and could not be elevated to dominance. In humans, the RBS is an immunogenic site that in principle can elicit bnAbs, within a group (e.g., CH65 [Whittle et al., 2011]) and in some cases, across groups (e.g., K03.12 [McCarthy et al., 2018], C05 [Ekiert et al., 2012]). Many of these human RBS-directed Abs engage the RBS through a relatively long CDR H3. Thus, a possible explanation for the failure to boost "canonical" RBS-directed Abs is that the average length of the CDR H3 in mice is 2–3 amino-acid residues shorter than in humans.

Pathogens use a variety of different mechanisms to subvert and avoid host immune surveillance. Chronic human pathogens such as HIV and hepatitis C viruses actively alter their glycoprotein glycan profiles to evade host immune recognition. A parallel can be made with influenza viruses if we consider them as chronic infections on the population level. The self-masking of the HIV Env through its glycan shield is thought to be a critical issue in eliciting bnAbs. Indeed, decoration (e.g., Sabouri et al., 2014; Reed et al., 2016) of foreign proteins with "self" glycans is widely thought to control immunogenicity such that only particulate antigens can activate humoral responses. However, we show that hyperglycosylating HA to create an equivalent glycan

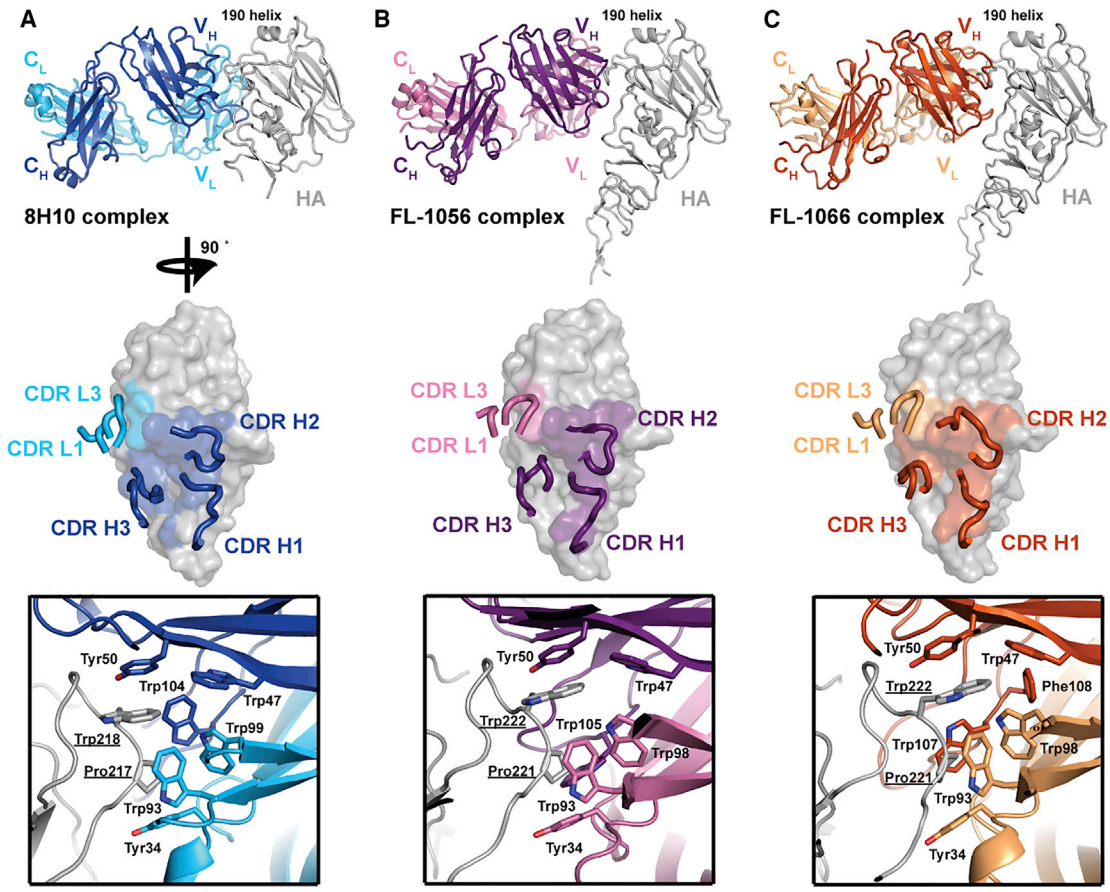

Figure 5. X-Ray Crystal Structures of V_H 5-9-1 Abs Show Convergence toward a Common Epitope

(A) Structure of 8H10 Fab bound with HA head of *v*H4 NB-10.

(B and C) Structures of (B) FL-1056 and (C) FL-1066 Fabs bound with HA head of WT H3 HK-68.

The top panels show the overall structures and indicate the immune focusing to a common epitope. The middle panels highlight the Fab footprints on HA and antibody CDR loops involved in binding. Contacts made by the CDR loops are detailed in the bottom panels. Essential HA residues are underlined. See also Figure S5; Table S1.

shield had no measurable effect on the overall magnitude of the primary serum Ab and GC responses. With no loss of immunogenicity, even the gHA^{shield} resulted in a redirection of specificity using restricted-gene usage. In short, the number of available epitopes did not appear to define the magnitude of humoral responses—an underlying assumption of the glycan shield model.

Immunogen design approaches for HIV have attempted to leverage glycosylation to selectively elicit bnAbs by removing glycans on HIV Env to expose epitopes targeted by bnAbs. The data presented here show seemingly the converse: adding glycans on influenza HA can change patterns of immunodominance and elicit broadly protective Abs. The template antigen in this study was the hypoglycosylated HK-68 HA and many of the engineered PNGs in our gHA immunogens derived from a naturally circulating, highly glycosylated H3 from 2011 (H3 Victoria/361/2011). An open question is whether, in the human population, those individuals exposed to circulating H3s since 2011 might have a higher frequency of Abs targeting the occluded epitope identified here (Watanabe et al., 2019).

How might the data from this study inform influenza vaccine strategies? Current immunogen design strategies for a universal influenza vaccine have focused primarily on how to elicit the subdominant, stem-directed Abs (Krammer and Palese, 2015). Like the murine Abs described here, human stem-directed Abs are also genetically restricted (primarily V_H1-69, in humans) and protect mice by Fc-dependent mechanisms. The similar properties of Abs directed at the head interface and the stem suggest that both may be useful components of a universal influenza vaccine; the hyperglycosylation strategy described here might be such an approach. Thus, by integrating immunogen design strategies that elicit both Fc-dependent (e.g., stem and/or head-interface) and neutralizing- (e.g., RBS) directed responses may lead to a broadly protective vaccine. The purpose of this study was to understand if there was an underlying, deterministic principle that dictates the immunodominance hierarchy. Our findings are that the magnitude of humoral responses, including serum antibody and the GC reaction, are little affected by a glycan shield. That is to say, the magnitude of overall humoral responses appears insensitive to the numbers of available epitopes on an immunogen. This observation suggests that the low immunogenicity of HIV and other variable antigens is not a consequence of "self-glycans" obscuring epitopes but rather other mechanisms (e.g., active

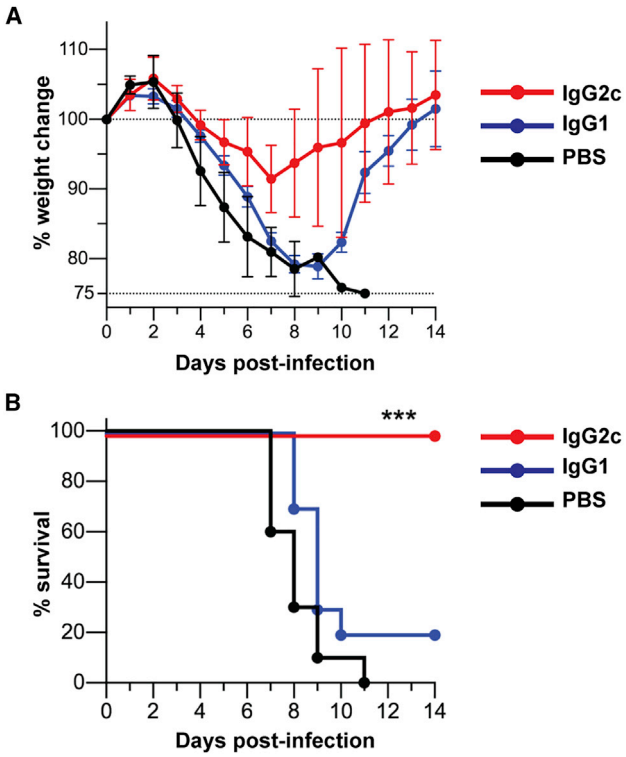

C

Virus	Endpoint Titer (μg/mL)	Positive Control Endpoint Titer
A/California/07/2009	> 50μg/mL	>10240
A/Aichi/1968 X-31	> 50μg/mL	1280
A/Wisconsin/67/2005	> 50μg/mL	10 μg/mL

Figure 6. V_H 5-9-1 Abs Are Non-neutralizing but Protect against a Viral Challenge through an Fc-Dependent Mechanism

Mouse challenge experiments were performed with intranasal viral infection ($5LD_{50}$) with X31-68 (H3N2) of mice injected with 100 μg of recombinant 8H10 as IgG2c or IgG1 isotype. (A total of 10 mice were used per group, including the PBS control.)

(A) The body-weight loss was monitored. (The error bars are the standard deviation of the weight of the survived mice starting with 10 mice for each group.)

(B) Kaplan-Meir survival curves of mice. The humane endpoint was set at 25% relative to the initial body weight, beyond which point the mice were euthanized. (The asterisks represent the statistical significance between PBS and IgG2c; the p value is 0.0003 calculated by log-rank [Mantel-Cox] test using Prism.)

(C) Microneutralization titers of 8H10 antibody are reported.

impairment of components of the immune system and host mimicry). Better understanding of this phenomenon can help focus and direct immune responses to desired epitope(s).

STAR★METHODS

Detailed methods are provided in the online version of this paper and include the following:

SUPPLEMENTAL INFORMATION

Supplemental Information can be found online at https://doi.org/10.1016/j.chom.2019.04.003.

ACKNOWLEDGMENTS

We thank Stephen Harrison at Harvard Medical School for helpful discussions. We thank Wenli Zhang, Dongmei Liao, Xiaoe Liang, Akiko Watanabe, Christopher Sample, and Ariel Mason for technical assistance. We thank Cees van der Poel for help with flow cytometry experiments and analyses. We thank the beamline staff at the Advanced Light Source (Lawrence Berkeley Laboratory), beamline 8.2.2, for assistance in recording of X-ray diffraction data and the NE-CAT staff members for advice and assistance in data collection. NE-CAT is funded by NIH grant P41 GM103403. APS is operated for the DOE Office of Science by Argonne National Laboratory under contract DE-AC02-06CH11357. Influenza stock propagation and microneutralization assays were done at the Virology Unit of the Duke Regional Biocontainment Laboratory (RBL), managed by C.E.M. and directed by G.D.S. The Duke RBL received partial support for construction from the National Institutes of Health, National Institute of Allergy and Infectious Diseases (UC6-AI058607). The following reagent was obtained through BEI Resources, NIAID, NIH: Polyclonal Anti-Influenza Virus, A/Aichi/2/1968 (H3N2), (antiserum, Guinea pig), NR-3126. Influenza A Virus, A/Wisconsin/67/2005 (H3N2), FR-397; Influenza A Virus, A/California/07/2009 (H1N1)pdm09 Antiviral Resistance (AVR) - Reference Virus M2: S31N NA: wt, FR-458; and Madin-Darby Canine Kidney (MDCK) Cells, London Line, FR-58, were obtained through the International Reagent Resource (formerly the Influenza Reagent Resource), Influenza Division, WHO Collaborating Center for Surveillance, Epidemiology and Control of Influenza, Centers for Disease Control and Prevention, Atlanta, GA, USA. Sequencing reactions were carried out with an ABI3730xl DNA analyzer at the DNA Resource Core of Dana-Farber/Harvard Cancer Center (funded in part by NCI Cancer Center support grant 2P30CA006516-48). The research was supported by AMED under grant number JP18fk0108051 (to Y.T.), NIH grants AI117892 and AI128832 (to G.K.) and AI089618 (to S.C. Harrison).

AUTHOR CONTRIBUTIONS

A.G.S. designed the research; G.B., M.J.M., Y.A., T.O., C.E.M., G.D.S., M.K., and A.G.S. performed research; G.B., M.J.M., Y.T., G.K., M.K., and A.G.S. analyzed data; A.G.S. wrote the paper: A.G.S. and G.B. prepared the figures; A.G.S, M.K., G.B., G.K., and M.J.M. edited and commented on the paper.

DECLARATION OF INTERESTS

The authors declare no competing interests.

Received: January 31, 2019
Revised: March 12, 2019
Accepted: April 8, 2019
Published: May 16, 2019

REFERENCES

Adams, P.D., Afonine, P.V., Bunkóczi, G., Chen, V.B., Davis, I.W., Echols, N., Headd, J.J., Hung, L.W., Kapral, G.J., Grosse-Kunstleve, R.W., et al. (2010). PHENIX: a comprehensive Python-based system for macromolecular structure solution. Acta Crystallogr. D Biol. Crystallogr. *66*, 213–221.

Bizebard, T., Gigant, B., Rigolet, P., Rasmussen, B., Diat, O., Bösecke, P., Wharton, S.A., Skehel, J.J., and Knossow, M. (1995). Structure of influenza virus haemagglutinin complexed with a neutralizing antibody. Nature *376*, 92–94.

Brochet, X., Lefranc, M.P., and Giudicelli, V. (2008). IMGT/V-Quest: the highly customized and integrated system for IG and TR standardized V-J and V-D-J sequence analysis. Nucleic Acids Res. *36*, W503–W508.

CDC. (2007). Influenza Virus Microneutralization Assay (Immunology and Pathogenesis Branch, Influenza Division, CDC United States Department of Health and Human Services).

CDC. (2009). Influenza Virus Microneutralization Assay H1N1 Pandemic Response (Centers for Disease Control, United States Department of Health and Human Services).

Chen, V.B., Arendall, W.B., 3rd, Headd, J.J., Keedy, D.A., Immormino, R.M., Kapral, G.J., Murray, L.W., Richardson, J.S., and Richardson, D.C. (2010). MolProbity: all-atom structure validation for macromolecular crystallography. Acta Crystallogr. D Biol. Crystallogr. *66*, 12–21.

Correia, B.E., Bates, J.T., Loomis, R.J., Baneyx, G., Carrico, C., Jardine, J.G., Rupert, P., Correnti, C., Kalyuzhniy, O., Vittal, V., et al. (2014). Proof of principle for epitope-focused vaccine design. Nature *507*, 201–206.

Corti, D., Voss, J., Gamblin, S.J., Codoni, G., Macagno, A., Jarrossay, D., Vachieri, S.G., Pinna, D., Minola, A., Vanzetta, F., et al. (2011). A neutralizing antibody selected from plasma cells that binds to group 1 and group 2 influenza A hemagglutinins. Science *333*, 850–856.

Crispin, M., Ward, A.B., and Wilson, I.A. (2018). Structure and immune recognition of the HIV glycan shield. Annu. Rev. Biophys.

Dreyfus, C., Laursen, N.S., Kwaks, T., Zuijdgeest, D., Khayat, R., Ekiert, D.C., Lee, J.H., Metlagel, Z., Bujny, M.V., Jongeneelen, M., et al. (2012). Highly conserved protective epitopes on influenza B viruses. Science *337*, 1343–1348.

Ekiert, D.C., Kashyap, A.K., Steel, J., Rubrum, A., Bhabha, G., Khayat, R., Lee, J.H., Dillon, M.A., O'Neil, R.E., Faynboym, A.M., et al. (2012). Cross-neutralization of influenza A viruses mediated by a single antibody loop. Nature *489*, 526–532.

Emsley, P., and Cowtan, K. (2004). Coot: model-building tools for molecular graphics. Acta Crystallogr. D Biol. Crystallogr. *60*, 2126–2132.

Fleury, D., Barrère, B., Bizebard, T., Daniels, R.S., Skehel, J.J., and Knossow, M. (1999). A complex of influenza hemagglutinin with a neutralizing antibody that binds outside the virus receptor binding site. Nat. Struct. Biol. *6*, 530–534.

Haynes, B.F., Kelsoe, G., Harrison, S.C., and Kepler, T.B. (2012). B-cell-lineage immunogen design in vaccine development with HIV-1 as a case study. Nat. Biotechnol. *30*, 423–433.

Jardine, J.G., Ota, T., Sok, D., Pauthner, M., Kulp, D.W., Kalyuzhniy, O., Skog, P.D., Thinnes, T.C., Bhullar, D., Briney, B., et al. (2015). HIV-1 vaccines. Priming a broadly neutralizing antibody response to HIV-1 using a germline-targeting immunogen. Science *349*, 156–161.

Kallewaard, N.L., Corti, D., Collins, P.J., Neu, U., McAuliffe, J.M., Benjamin, E., Wachter-Rosati, L., Palmer-Hill, F.J., Yuan, A.Q., Walker, P.A., et al. (2016). Structure and function analysis of an antibody recognizing all influenza A subtypes. Cell *166*, 596–608.

Kepler, T.B. (2013). Reconstructing a B-cell clonal lineage. I. Statistical inference of unobserved ancestors. F1000Res *2*, https://doi.org/10.12688/f1000research.2-103.v1.

Krammer, F., and Palese, P. (2015). Advances in the development of influenza virus vaccines. Nat. Rev. Drug Discov. *14*, 167–182.

Krause, J.C., Tsibane, T., Tumpey, T.M., Huffman, C.J., Basler, C.F., and Crowe, J.E., Jr. (2011). A broadly neutralizing human monoclonal antibody that recognizes a conserved, novel epitope on the globular head of the influenza H1N1 virus hemagglutinin. J. Virol. *85*, 10905–10908.

Kuraoka, M., Schmidt, A.G., Nojima, T., Feng, F., Watanabe, A., Kitamura, D., Harrison, S.C., Kepler, T.B., and Kelsoe, G. (2016). Complex antigens drive permissive clonal selection in germinal centers. Immunity *44*, 542–552.

Lavie, M., Hanoulle, X., and Dubuisson, J. (2018). Glycan shielding and modulation of hepatitis C virus neutralizing antibodies. Front. Immunol. *9*, 910.

Mascola, J.R., and Haynes, B.F. (2013). HIV-1 neutralizing antibodies: understanding nature's pathways. Immunol. Rev. *254*, 225–244.

McCarthy, K.R., Watanabe, A., Kuraoka, M., Do, K.T., McGee, C.E., Sempowski, G.D., Kepler, T.B., Schmidt, A.G., Kelsoe, G., and Harrison, S.C. (2018). Memory B cells that cross-react with Group 1 and Group 2 influenza A viruses are abundant in adult human repertoires. Immunity *48*, 174–184.

McCoy, A.J., Grosse-Kunstleve, R.W., Adams, P.D., Winn, M.D., Storoni, L.C., and Read, R.J. (2007). Phaser crystallographic software. J. Appl. Crystallogr. *40*, 658–674.

Modis, Y., Ogata, S., Clements, D., and Harrison, S.C. (2003). A ligand-binding pocket in the dengue virus envelope glycoprotein. Proc. Natl. Acad. Sci. USA *100*, 6986–6991.

Modis, Y., Ogata, S., Clements, D., and Harrison, S.C. (2005). Variable surface epitopes in the crystal structure of dengue virus type 3 envelope glycoprotein. J. Virol. *79*, 1223–1231.

Murshudov, G.N., Skubák, P., Lebedev, A.A., Pannu, N.S., Steiner, R.A., Nicholls, R.A., Winn, M.D., Long, F., and Vagin, A.A. (2011). REFMAC5 for the refinement of macromolecular crystal structures. Acta Crystallogr. D Biol. Crystallogr. *67*, 355–367.

Ofek, G., Guenaga, F.J., Schief, W.R., Skinner, J., Baker, D., Wyatt, R., and Kwong, P.D. (2010). Elicitation of structure-specific antibodies by epitope scaffolds. Proc. Natl. Acad. Sci. USA *107*, 17880–17887.

Petrova, V.N., and Russell, C.A. (2018). The evolution of seasonal influenza viruses. Nat. Rev. Microbiol. *16*, 60.

Reed, J.H., Jackson, J., Christ, D., and Goodnow, C.C. (2016). Clonal redemption of autoantibodies by somatic hypermutation away from self-reactivity during human immunization. J. Exp. Med. *213*, 1255–1265.

Reynolds, A.E., Kuaoka, M., and Kelsoe, G. (2015). Natural IgM is produced by CD5- plasma cells that occupy a distinct survival niche in bone marrow. J Immunol. *194*, 231–242.

Schmidt, A.G., Do, K.T., McCarthy, K.R., Kepler, T.B., Liao, H.X., Moody, M.A., Haynes, B.F., and Harrison, S.C. (2015a). Immunogenic stimulus for germline precursors of antibodies that engage the influenza hemagglutinin receptor-binding site. Cell Rep. *13*, 2842–2850.

Schmidt, A.G., Therkelsen, M.D., Stewart, S., Kepler, T.B., Liao, H.X., Moody, M.A., Haynes, B.F., and Harrison, S.C. (2015b). Viral receptor-binding site antibodies with diverse germline origins. Cell *161*, 1026–1034.

Sabouri, Z., Schofield, P., Horikawa, K., Spierings, E., Kipling, D., Randall, K.L., Langley, D., Roome, B., Vazquez-Lombardi, R., Rouet, R., et al. (2014). Redemption of autoantibodies on anergic B cells by variable-region glycosylation and mutation away from self-reactivity. Proc. Natl. Acad. Sci. USA *111*, E2567–E2575.

Watanabe, A., McCarthy, K.R., Kuraoka, M., Schmidt, A.G., Adachi, Y., Onodera, T., Tonouchi, K., Caradonna, T.M., Bajic, G., Song, S., et al.

(2019). Antibodies to a conserved influenza head interface epitope protect by an IgG subtype-dependent mechanism. Cell *177*, https://doi.org/10.1016/j.cell.2019.03.048.

Watanabe, Y., Raghwani, J., Allen, J.D., Seabright, G.E., Li, S., Moser, F., Huiskonen, J.T., Strecker, T., Bowden, T.A., and Crispin, M. (2018). Structure of the Lassa virus glycan shield provides a model for immunological resistance. Proc. Natl. Acad. Sci. USA *115*, 7320–7325.

Whittle, J.R., Zhang, R., Khurana, S., King, L.R., Manischewitz, J., Golding, H., Dormitzer, P.R., Haynes, B.F., Walter, E.B., Moody, M.A., et al. (2011). Broadly neutralizing human antibody that recognizes the receptor-binding pocket of influenza virus hemagglutinin. Proc. Natl. Acad. Sci. USA *108*, 14216–14221.

WHO. (2010). Serological Diagnosis of Influenza by Microneutralization Assay (World Health Organization).

WHO. (2011). Manual for the Laboratory Diagnosis and Virological Surveillance of Inflluenza (World Health Organization).

Winn, M.D., Ballard, C.C., Cowtan, K.D., Dodson, E.J., Emsley, P., Evans, P.R., Keegan, R.M., Krissinel, E.B., Leslie, A.G., McCoy, A., et al. (2011). Overview of the CCP4 suite and current developments. Acta Crystallogr. D Biol. Crystallogr. *67*, 235–242.

Wrammert, J., Smith, K., Miller, J., Langley, W.A., Kokko, K., Larsen, C., Zheng, N.Y., Mays, I., Garman, L., Helms, C., et al. (2008). Rapid cloning of high-affinity human monoclonal antibodies against influenza virus. Nature *453*, 667–671.

STAR★METHODS

KEY RESOURCES TABLE

REAGENT or RESOURCE	SOURCE	IDENTIFIER
Antibodies		
FITC Rat anti-mouse GL-7 antibody (GL7)	BD Biosciences	CAT#553666
PE Rat anti-mouse CD138 antibody (281-2)	BD Biosciences	CAT#553714
PE/Cy7 Rat anti-mouse CD38 antibody (90)	BioLegend	CAT#102718
APC Rat anti-mouse CD93 antibody (AA4.1)	BioLegend	CAT#136510
Brilliant Violet 421 Rat anti-mouse B220 antibody (RA3-6B2)	BioLegend	CAT#103240
Brilliant Violet 510 Rat anti-mouse IgD antibody (11-26C.2a)	BD Biosciences	CAT#563110
A488 goat anti-human IgG H+L	Thermo Scientific	CAT#A11013
Ferret hyperimmune sera to A/California/07/2009 (H1N1)	BEI Resources, NIAID, NIH	CAT#NR-19261
Polyclonal Anti-Influenza Virus, A/Aichi/2/1968 (H3N2)	BEI Resources, NIAID, NIH	CAT# NR-3126
PE conjugated goat anti-mouse IgG	Southern Biotech	CAT#1030-09
Goat anti-mouse IgG-HRP	Southern Biotech	CAT#1030-05
Goat anti-mouse kappa UNLB	Southern Biotech	CAT#1050-01
Goat anti-mouse lambda UNLB	Southern Biotech	CAT#1060-01
anti-human IgG-HRP	Abcam	ab97225
Mouse anti-Human IgG G18-145 BB515 conjugated	BD Horizon	CAT#564581
Bacterial and Virus Strains		
A/Aichi/2/1968 X-31 (H3N2)	Charles River Avian Vaccine Services	CAT#10100375
A/Aichi/2/1968 X-31 (H3N2)	Takeshi Tsubata (Tokyo Medical and Dental University)	N/A
Biological Samples		
Fetal Bovine serum (HyClone)	Thermo Scientific	SH30070.03
Fetal Bovine serum, ultra-low IgG	Thermo Scientific	CAT#16250078
Chemicals, Peptides, and Recombinant Proteins		
Pierce HRV 3C Protease	ThermoFisher	CAT#88946
TALON Metal Affinity Resin	Clontech	CAT#635652
Pierce Protein G Agarose	ThermoFisher	CAT# 20399
Polyethylenimine, Linear, MW 25000, Transfection Grade	Poly Sciences	CAT# 23966-1
1-Step ABTS substrate	ThermoFisher	Prod#37615
Fixation Buffer	Biolegend/VWR	CAT#420801-BL
Recombinant mouse IL-4	Peprotech	CAT#214-14
eFluor 780 Fixable Viability Dye	Thermo Scientific	CAT#65-0865-14
Deposited Data		
Atomic coordinates, 8H10 HA complex	Protein Data Bank	PDB: 6N5B
Atomic coordinates, FL-1056 HA complex	Protein Data Bank	PDB: 6N5D
Atomic coordinates, FL-1066 HA complex	Protein Data Bank	PDB: 6N5E
Experimental Models: Cell Lines		
Human: Gibco 293-F	ThermoFisher	CAT# 11625019
Human: Expi293F	ThermoFisher	CAT# A14527

(*Continued on next page*)

Continued

REAGENT or RESOURCE	SOURCE	IDENTIFIER
Human: HEK293S GnTI-/-	ATCC	ATCC CRL-3022
S. frugiperda: Sf9	ThermoFisher	CAT# 11496015
T. ni: High Five	ThermoFisher	CAT#B85502
NB-21.2D9	Kuraoka et al., 2016	N.A.
Experimental Models: Organisms/Strains		
C57BL/6J mouse	The Jackson Laboratory	CAT#000664
C57BL/6J mouse	Japan SLC	C57BL/6JJmsSlc
Recombinant DNA		
pVRC_8H10 _HC_3C_His_Fab	This study	N/A
pVRC_8H10 _LC	This study	N/A
pVRC_8H10 _HC_human_IgG	This study	N/A
pVRC_8H10 _HC_murine_IgG1	This study	N/A
pVRC_8H10 _HC_murine_IgG2c	This study	N/A
pVRC_FL-1056 _HC_3C_His_Fab	This study	N/A
pVRC_FL-1056 _LC	This study	N/A
pVRC_FL-1056 _HC_murine_IgG1	This study	N/A
pVRC_FL-1066 _HC_3C_His_Fab	This study	N/A
pVRC_FL-1066 _LC	This study	N/A
pVRC_FL-1066 _HC_murine_IgG2	This study	N/A
pVRC_FL-1066 _HC_human_IgG1	This study	N/A
pVRC_ HC19_human_ HC_IgG	Bizebard et al., 1995	N/A
pVRC_ HC19_human_ HC_Fab	Bizebard et al., 1995	N/A
pVRC_ HC19_human_LC	Bizebard et al., 1995	N/A
pVRC_ MEDI8852_human_ HC_IgG	Kallewaard et al. 2016	N/A
pVRC_ MEDI8852_human_ LC	Kallewaard et al. 2016	N/A
pVRC_ CR9114_human_ HC_IgG	Dreyfus et al. 2012	N/A
pVRC_ CR9114_human_ LC	Dreyfus et al., 2012	N/A
pVRC_FI6v3_IgG	Corti et al., 2011	N/A
pVRC_FI6v3_LC	Corti et al., 2011	N/A
pVRC_ HC45_human_HC_IgG	Fleury et al., 1999	N/A
pVRC_ HC45_human_LC	Fleury et al., 1999	N/A
pVRC_CH67_human_HC_IgG	Schmidt et al., 2015a	N/A
pVRC_CH67_human_LC	Schmidt et al., 2015a	N/A
pVRC_X31_FLsE_gHA_RBS	This study	N/A
pVRC_X31_FLsE_gHA_cRBS	This study	N/A
pVRC_X31_FLsE_gHA_shield	This study	N/A
pFB_H1_Solomon_Islands_2006_FLsE	Whittle et al., 2011	N/A
pFB_H3_Aichi_2_1968_(X31)_FLsE	This study	N/A
pFB_H3_Aichi_2_1968_(X31)_head	This study	N/A
pFB_H3_Port_Chalmers_1973_FLsE	This study	N/A
pFB_H3_Victoria_1975_FLsE	This study	N/A
pFB_H3_Texas_1977_FLsE	This study	N/A
pFB_H3_Philippines_2_1982_FLSE	This study	N/A
pFB_H3_Leningrad_360_1986_FLSE	This study	N/A
pFB_H3_Shanghai_1987_FLsE	This study	N/A
pFB_H3_Beijing_353_1989_FLsE	This study	N/A
pFB_H3_Johannesburg_33_1994_FLsE	This study	N/A
pFB_H3_Moscow_10_1999_head	This study	N/A
pFB_H3_Wisconsin_67_2005_FLsE	This study	N/A

(*Continued on next page*)

Continued

REAGENT or RESOURCE	SOURCE	IDENTIFIER
pFB_H4_New Brunswick_2010_FLsE	This study	N/A
pFB_H4_New Brunswick_2010_head	This study	N/A
pFB_variant_H4_New Brunswick_2010_head	This study	N/A
pVRC_H3_Aichi_2_68_(X31)_FLsE	This study	N/A
pVRC_H4_New Brunswick_10_FLsE	This study	N/A
pVRC_variant_H4_New Brunswick_10_head	This study	N/A
Software and Algorithms		
FlowJo	Treestar Inc	https://www.flowjo.com/
FACSDIVA	BD Biosciences	http://www.bdbiosciences.com/us/instruments/research/software/flow-cytometry-acquisition/bd-facsdiva-software/m/111112/overview
PHASER	McCoy et al., 2007	http://www.phaser.cimr.cam.ac.uk/index.php/Phaser_Crystallographic_Software
Coot	Emsley and Cowtan, 2004	http://www2.mrc-lmb.cam.ac.uk/personal/pemsley/coot/
PHENIX	Adams et al., 2010	https://www.phenix-online.org/
PyMol	Schrödinger	http://www.pymol.org
MolProbity	Chen et al., 2010	http://molprobity.biochem.duke.edu
REFMAC5	Murshudov et al., 2011	http://www.ccp4.ac.uk/dist/html/refmac5.html
Clonalyst	Kepler, 2013	http://www.bu.edu/computationalimmunology/research/software/
IMGT/V-QUEST	Brochet et al., 2008	http://www.imgt.org/IMGT_vquest/vquest
FlowJo	FlowJo	https://www.flowjo.com/
Prism 8	GraphPad Software	https://www.graphpad.com/scientific-software/prism/
Other		
Pathogen Free embryonated chicken eggs	Sunrise Farms or Charles River Avian Vaccine Services	CAT#10100326
FreeStyle 293 Expression Medium	Thermo Scientific	CAT#12338018
Expi293 Expression Medium	Thermo Scientific	CAT# A1435101
Sf-900 II SFM	Thermo Scientific	CAT# 10902096
EX-CELL 405 Serum-Free Medium	Sigma	CAT# 14405C

CONTACT FOR REAGENT AND RESOURCE SHARING

Further information and requests for resources and reagents should be directed to and will be fulfilled by the Lead Contact, Aaron G. Schmidt (aschmidt@crystal.harvard.edu).

EXPERIMENTAL MODEL

Mice

C57BL/6J (female, age 7 to 12-week-old) mice were obtained from the Jackson Laboratory and from Japan SLC and maintained under specific pathogen-free conditions at the Duke University Animal Care Facility and the National Institute of Infectious Diseases (NIID), respectively. At Duke University, the mice were housed in a temperature-controlled (68-72 °F), air-conditioned room on a 12-hr light-dark cycle. The mice were supplied corn cob bedding (1/4-inch depth), reversed osmosis water and Purim's 5053 as standard diet. At NIID, all mice were maintained in an SPF condition, provided with water, and a standard laboratory diet (FR-2, Funabashi Farm Co.,Ltd.). They were supplied with hardwood chips as bedding and housed in a temperature-controlled, air-conditioned room on a 12-hr light-dark cycle. For infection studies, mice were maintained in BSL2 facility under the same housing conditions. All experiments (except for protection studies) involving animals were approved by the Duke University Institutional Animal Care and Use Committee. Protection studies were approved by the Animal Ethics Committee of the National Institute of Infectious Diseases, Japan, and performed in accordance with the guidelines of the Institutional Animal Care and Use Committee.

Cell Lines

High Five Cells (BTI-TN-5B1-4, female) (*Trichoplusia ni*) were maintained at 28° degrees Celsius in EX-CELL 405 serum-free medium (Sigma) supplemented with penicillin and streptomycin. Sf9 cells (*Spodoptera frugiperda*, female) were maintained at 28° degrees Celsius in Sf-900™ II SFM media. Human embryonic kidney cells (HEK, presumed female) 293F cells were maintained at 37° degrees Celsius with 5% CO_2 in FreeStyle 293 media (ThermoFisher) supplemented with penicillin and streptomycin. Human HEK293S GnTI-/- suspension cell cultures, (presumed female) maintained in FreeStyle 293 expression medium supplemented with 2% FBS supplemented with penicillin and streptomycin at 37° degrees Celsius with 5% CO_2. Madin-Darby canine kidney cells (MDCK) (*Canis lupus familiaris*, Cocker Spaniel, female) were maintained in DMEM at 37° degrees Celsius with 5% CO_2. Cell lines were not subject to authentication. NB-21.2D9 cells (derived from BALB/c 3T3 fibroblasts, female, Kuraoka et al. Immunity 2016) were maintained at 37° degrees Celsius with 5% CO_2 in DMEM (Invitrogen) supplemented with penicillin and streptomycin (Invitrogen), non-essential amino acids (NEAA, Invitrogen), and 10% FBS (HyClone, ThermoFisher).

METHOD DETAILS

HA Expression and Purification

rHA "head" and rHA full length soluble ectodomains (FLsE) constructs were cloned into pFastBac vector for insect cell expression (Hi5 cells) or pVRC vector for mammalian expression (293F or 293S cells). All constructs were confirmed by DNA sequencing at the DNA Sequencing Core Facility at Dana Farber Cancer Institute. For biolayer interferometry (BLI) and crystallography the HA1 head constructs contained a HRV 3C-cleavable C-terminal His_{6X} tag or SBP-His_{8X}tag. The HA FLsE constructs used in ELISA assays contained a thrombin or HRV 3C-cleavable C-terminal foldon tag with either a His_{6X} or SBP-His_{8X}tag. All constructs were purified from supernatants by passage over Cobalt-TALON resin (Takara) followed by gel filtration chromatography on Superdex 200 Increase (GE Healthcare) in 10 mM Tris-HCl, 150 mM NaCl at pH 7.5. Affinity tags were removed using HRV 3C protease (ThermoScientific) and the protein repurified using Cobalt-TALON resin to remove the protease, tag and non-cleaved protein.

Fab and IgG Expression and Purification

For Fab and IgG production the genes for the heavy- and light-chain variable domains were synthesized and codon optimized by Integrated DNA Technologies and subcloned into pVRC protein expression vectors containing human heavy- and light-chain constant domains ((Schmidt et al., 2015a; Schmidt et al., 2015b)). Constructs were confirmed by sequencing at the DNA Sequencing Core Facility at Dana Farber Cancer Institute. Fabs and IgGs were produced by transient transfection in suspension 293F cells using polyethylenamine (PEI). Supernatants were harvested 4-5 days later, clarified by centrifugation. Fabs were purified using Cobalt-TALON resin (Takara) followed by gel filtration chromatography on Superdex 200 Increase (GE Healthcare) in 10 mM Tris-HCl, 150 mM NaCl at pH 7.5. IgGs were purified using Protein G Plus Agarose (ThermoFisher Scientific). Briefly, IgG supernatants were incubated overnight with agarose slurry, eluted with 0.1M glycine, pH 2.5 and normalized with 1M Tris-HCl, pH 8.0 and dialyzed against PBS buffer overnight.

ELISA

5-10ng of rHA FLsE were adhered to high-capacity binding, 96 well-plates (Corning) overnight in PBS. Plates were blocked with non-fat dried milk in PBS containing Tween-20 (PBS-T) for 1hr at room temperature (RT). Blocking solution was discarded and 10-fold dilutions of RBS-directed IgGs in PBS were added to wells and incubated for 1hr at RT. Plates were then washed three times with PBS-T. Secondary, anti-human IgG-HRP (Abcam), in PBS-T was added to each and incubated for 1hr at RT. Plates were then washed three times with PBS-T. Plates were developed using 1-Step ABTS substrate (ThermoFisher) and immediately read using a plate reader at 410nm. Data were plotted using Prism 6 (GraphPad Software) and affinities determined. For intact virion binding, the 96 well-plates were coated (in two replicates) with 50 μl of H3N2 A/Aichi/2/1968 (X31) virus (Charles River) at 10 μg/ml for 2 hours at room temperature (RT) in PBS. Plates were blocked with 2% BSA in PBS for 1 hour at RT. Blocking solution was discarded and triplicates of 5-fold dilutions of human IgG1 mAbs HC19, FI6v3 and FL-1066 in blocking solution were added to wells and incubated for 1hr at RT. Plates were then washed three times with PBS. Secondary, anti-human IgG-HRP (1:10000 dilution, Abcam 97225), in PBS was added and incubated for 30 min at RT. Plates were then washed three times with PBS and developed using 1-Step Ultra TMB substrate (ThermoFisher) The reaction stopped with 2M sulfuric acid and absorbance at 450nm read using a plate reader.

Cell-Surface HA Staining

Human HEK293S cells were transiently transfected with the modified pVRC8400 expression vectors into which full-length HAs were cloned (Schmidt et al., 2015b) using polyethylenimine (PEI). Transfection complexes were prepared in Opti-MEM and added to cells. At 24 hours post transfection, cells were harvested for staining. The cells were pelleted at 200 g and washed with phosphate buffered saline (PBS) pH 7.4 supplemented with 1mM EDTA, 0.5% BSA (FACS buffer). 50,000 cells were then incubated for 30 minutes on ice with primary antibody (human IgG1) at a range of concentrations 0.045-100nM in FACS buffer. Cells were washed three times in FACS buffer and incubated with goat anti-human IgG antibody conjugated with A488 (1:500 dilution, Thermo Scientific CAT#A11013) and eFluor® 780 Fixable Viability Dye (1:2000 dilution, Thermo Scientific CAT#65-0865-14) for 30 minutes on ice. The cells were washed and resuspended in the FACS buffer. Fluorescence was measured using a BD FACSCanto equipped with HTS and analyzed using FlowJo software (FlowJo Inc, Ashland, OR).

Crystallization and Data Collection

A/Hong Kong/1/1968-X31 (H3N2) HA1 head domain and FL-1056 or FL-1066 Fab were incubated at 1:1.5 molar ratio, respectively. An engineered variant of H4 A/American black duck/New Brunswick/00464/2010 (*v*H4 NB-10) was pre-incubated with 8H10 Fab at 1:1.3 molar excess. The complexes were isolated by size exclusion chromatography using a 24 mL Superdex Increase equilibrated in 10 mM Tris-HCl, 150 mM NaCl. Crystallization was achieved by hanging drop vapor diffusion at 18°C. 8H10 complex crystals were grown in 0.1M MES pH 6.5, 12% PEG 20000; FL-1056 complex in 0.2 M Sodium bromide, 0.1 M Bis-Tris propane 6.5, 20 % w/v PEG 3350 and FL-1066 complex in 0.2 M ammonium sulfate, 0.1 M MES pH 6.5, 20 % w/v PEG 8000. Crystals were cryoprotected in mother liquor supplemented with 10% MPD or 20% (vol/vol) glycerol and flash-frozen in liquid nitrogen. Data were collected at 0.999 Å with a rotation of 1° per image on the 8.2.2 beamline, Advanced Light Source., at Berkley National Laboratory.

Data Processing, Structure Determination and Refinement

Processing of single-crystal X-ray diffraction data was done with the XDS software package. For the 8H10 complex, the data were scaled in the $P3_121$ space group and the structure determined with molecular replacement (MR) in PHASER using H4 A/Duck/Czechoslovakia/1956 (PDB 5XL3) for the HA "head" and for the murine Fab the V_H, V_L (PDB 2QHR, 1GIG, respectively) and C_H, C_L (PDB 2VIR) as search models. The *v*H4 NB-10 head used for crystallization had mutations in the receptor-binding site periphery; these regions were rebuilt from the starting model. The structure was then refined with phenix.refine using, group B factor and Translation Libration Screw-rotation (TLS) refinement. There was strong density for the HA head except in the extreme N and C-termini where there appeared to be flexibility; the density did not improve during refinement and these regions were omitted from the final model. For the FL-1056 and FL-1066 complexes, the data were initially scaled in the $P3_112$ space group but solving the phase problem with MR failed. Twinning by merohedry became apparent after data analysis by phenix.xtriage; the estimated twin fraction was 0.395 and the twin law –k,-h,-l. The data were then scaled in the $P3_1$ space group and detwinned with the program DETWIN from the CCP4 program suite (Winn et al., 2011). The structures were determined by MR using PHASER (McCoy et al., 2007) with the A/Hong Kong/1/1968-X31 head domain (PDB ID 1HA0) and 8H10 Fab as search model. Structure refinement was performed with phenix.refine (Adams et al., 2010) using twin refinement, individual B factor and real-space refinement and REFMAC5 (Murshudov et al., 2011) using twin refinement, isotropic B factor and jelly-body refinement. Model building was done in COOT (Emsley and Cowtan, 2004) and assessed with MolProbity (Chen et al., 2010). N-linked glycan stereochemistry was validated with Privateer. Figures were generated using PyMOL Molecular Graphics System (v1.8.0.0; Schrödinger LLC).

Murine Immunizations and Protection Studies

For immunizations, mice were immunized with 20 μg of rHAs (see above) in alum or in Alhydrogel® adjuvant 2% (InvivoGen) via footpad. For protection studies, 7 to 12-week-old female mice were injected *i.p.* with 100 μg of 8H10 recombinant antibody or PBS in 200 μl and three hours later, they were anesthetized by sodium pentobarbital and infected intranasally by $5LD_{50}$ of X31-68 (H3N2) in 50 μl volumes. Mice were monitored daily for survival and body weight loss until 14 days after challenge. The humane endpoint was set at 25% body weight loss relative to the initial body weight at the time of infection.

Flow Cytometry

GC B cells (GL-7$^+$B220^{hi}CD38^{lo}IgD$^-$CD93$^-$CD138$^-$) and plasmablasts/-cytes (B220^{lo}CD138^{hi}) cells in popliteal LNs were determined as described (Reynolds et al., 2015; Kuraoka et al., 2016). Labeled cells were analyzed/sorted in a FACS Canto (BD Bioscience) or a FACS Vantage with DIVA option (BD Bioscience). Flow cytometric data were analyzed with FlowJo software (Treestar Inc.). Doublets were excluded by FSC-A/FSC-H gating strategy. Cells that took up propidium iodide were excluded from our analyses.

Nojima Cultures

Single B cell cultures were performed as described (Kuraoka et al., 2016). Briefly, single GC B cells were cultured for 10 days in the presence of NB-21.2D9 feeder cells. After culture, culture supernatants were harvested for Luminex determinations and culture plates were stored at -80°C for V(D)J amplifications.

Luminex Multiplex Assay

Reactivity of clonal IgGs in culture supernatants and mouse sera was determined by Luminex multiplex assay (Kuraoka et al., 2016; McCarthy et al., 2018). Mixtures of antigen-conjugated microspheres were incubated with 1:10 diluted culture supernatant samples or with serially diluted serum samples for 2 hours at room temperature with mild agitation. Samples were diluted in PBS containing 1% cow milk, 1% BSA, 0.05% Tween 20 and 0.05% NaN_3. After washing, PE goat anti-mouse IgG (Southern Biotech) was added to the plates and incubated for 1 hour at room temperature with mild agitation. After washing, microspheres were resuspended in PBS containing 1% BSA, 0.05% Tween 20 and 0.05% NaN_3 and fluorescent signals from each microsphere were measured in a Bio-Plex® 3D machine (Bio-Rad).

BCR Repertoire Analysis

V(D)J rearrangements of cultured B cells were amplified by a nested PCR, cloned, and sequenced as previously described (Kuraoka et al., 2016). The rearranged V, D, and J gene segments were identified using IMGT/V-QUEST (http://www.imgt.org/) or Cloanalyst (Kepler, 2013).

Influenza Microneutralization Assay

Virus neutralization endpoint titers (EPT) were determined using the influenza microneutralization assay as described (CDC, 2007, 2009; McCarthy et al., 2018; WHO, 2010, 2011). Monoclonal antibodies were diluted to test concentration in assay diluent and evaluated as duplicate, two-fold dilutions series. Absorbance was measured using a Synergy H1 microplate reader (BioTek Instruments Inc., Winooski, Vermont). Influenza viruses were propagated in embryonated specific-pathogen-free chicken hen eggs or MDCK (CCL-34) cells as previously described (McCarthy et al., 2018).

QUANTIFICATION AND STATISTICAL ANALYSIS

Binding Studies

Affinity dissociation constant (K_D) values for ELISA (see Figure S4A legend) were obtained as follows. All dilutions were done in duplicate, for two independent assays (n=2). The average background signal (no primary antibody) was subtracted from all absorbance values. Values from multiple plates were normalized to the MEDI8852 standard that was present on each ELISA plate. The mean values of the two measurements were then graphed using GraphPad Prism (v8.0.2.) and the standard deviation (SD) shown. K_D values were determined by applying a non-linear fit (One site – Total binding) to these data points. For intact virion binding, all dilutions were done in triplicate, for two independent assays (n=2). The mean values of the three measurements were then graphed using GraphPad Prism (v8.0.2.) and their standard deviation shown (see Figure S4D legend).

Immunizations

Immunizations were done using wildtype H3 H3X31 (n=5, 7), gHA^{RBS} (n=4, 6), gHA^{cRBS} (n=4, 6) and gHA^{shield} (n=2, 4); n = number of mice used for day 8, 16 analyses, respectively. In Figure 2, serum analyses include all mice from day 16 from each immunization. In Figures S2E and S2F one lymph node (LN) per mouse was used; n= number of mice.

In Vivo Protection Experiments

A total of thirty mice were used for the *in vivo* protection experiments with ten mice (n=10) used for the IgG1, IgG2c and PBS-control. Statistical significance of body weight change and survival of mice after lethal influenza challenge was calculated by Two-way ANOVA test and Mantel-Cox test, respectively, using GraphPad Prism (v8.0.2.) software (see Figure 6 legend and Method Details).

Statistical Analyses

Software used for statistical analyses described were done using GraphPad Prism (v8.0.2.). Additional software for analysis include FlowJo software (Treestar Inc.) for flow cytometry.

DATA AND SOFTWARE AVAILABILITY

The accession numbers for the coordinates and structure factors reported in this paper are PDB: 6N5B, 6N5D, and 6N5E.